論文 / 著書情報
Article / Book Information

Title	Weakly guiding approximation of a three dimensional waveguide model for extreme ultraviolet lithography simulation
Authors	Hiroyoshi Tanabe, Akira Jinguji, Atsushi Takahashi
Citation	Journal of the Optical Society of America A, Vol. 41, Issue 8, pp. 1491-1499
Pub. date	2024, 7
Copyright	(c) 2024 Optica Publishing Group. Users may use, reuse, and build upon the article, or use the article for text or data mining, so long as such uses are for non-commercial purposes and appropriate attribution is maintained. All other rights are reserved.
DOI	http://dx.doi.org/10.1364/JOSAA.516610

Research Article Vol. 41, No. 8 / August 2024 / Journal of the Optical Society of America A 1491

Journal of the Optical Society of America A

OPTICS, IMAGE SCIENCE, AND VISION

Weakly guiding approximation of a three-dimensional waveguide model for extreme ultraviolet lithography simulation

HIROYOSHI TANABE,* AKIRA JINGUJI, AND ATSUSHI TAKAHASHI

Tokyo Institute of Technology, 2-12-1 Ookayama, Meguro-ku, Tokyo 152-8550, Japan
**tanabe.h.af@m.titech.ac.jp*

Received 20 December 2023; revised 27 May 2024; accepted 11 June 2024; posted 12 June 2024; published 8 July 2024

A three-dimensional (3D) waveguide model is applied in extreme ultraviolet (EUV) lithography simulations. The 3D waveguide model is equivalent to rigorous coupled-wave analysis, but fewer field components are used to solve Maxwell's equations. The 3D waveguide model uses two components of vector potential, A_x and A_y, corresponding to the two polarizations. The electric field of the A_x polarization is approximately parallel to the x axis, and the electric field of the A_y polarization is approximately parallel to the y axis. The 3D waveguide model solves a coupled vector wave equation for two polarizations. The refractive index of conventional EUV absorbers is close to that of vacuum. The weakly guiding approximation in optical fiber theory is applied to the 3D waveguide model. The coupled vector wave equations for the two polarizations are decoupled into two independent scalar wave equations. Maxwell's equations are simplified to a set of scalar wave equations. The weakly guiding approximation reduces the computation time to solve the equations. The computation time required to solve the weakly guiding approximation is about 1/5 of the time to solve the original 3D waveguide model.

https://doi.org/10.1364/JOSAA.516610

1. INTRODUCTION

Extreme ultraviolet (EUV) lithography has begun to be used in the mass production of logic and memory devices. The typical resolution for EUV lithography is 16 nm assuming a numerical aperture (NA) of 0.33 and a moderate k_1 factor of 0.4. In this case, the minimum size of the mask pattern will be 64 nm. The typical thickness of the Ta absorber is about 60 nm, and the aspect ratio of the mask pattern is nearly 1. High-aspect absorbers give rise to several mask three-dimensional (3D) effects, such as critical dimension differences between horizontal and vertical lines and focus-dependent pattern shift [1,2]. Accurate electromagnetic (EM) simulation is required to reproduce these mask 3D effects.

There are two types in EM simulation methods. The finite-difference time-domain (FDTD) method [3] solves Maxwell's equations in coordinate space, and the solution is the near-field diffraction amplitude. Since the near-field diffraction amplitude depends on the incident angle, the calculation must be repeated for all source points (usually 100 or more).

On the other hand, rigorous coupled-wave analysis (RCWA) [4–7] and the 3D waveguide model [8,9] solve Maxwell's equation in momentum (or frequency) space. Assuming a periodic boundary condition, the momentum is discretized proportional to the inverse of the period length. These models solve a coupled-wave equation that connects the incoming and outgoing waves. All relationships between the incoming and outgoing waves are calculated simultaneously. The momentum of the incoming wave corresponds to the source position. If the period length is large enough, the size of the momentum grid is small, and these models do not need to repeat calculations for different source points.

The formulations of RCWA and the 3D waveguide model are equivalent as shown in Appendix A of this paper. The difference between the two approaches is the number of the field components used in solving Maxwell's equations. The RCWA method uses four components of electric and magnetic fields: E_x, E_y, H_x and H_y. On the other hand, the 3D waveguide model uses two field components: vector potentials A_x and A_y.

Maxwell's equations contain six field components, the electric field $\boldsymbol{E}$, and the magnetic field $\boldsymbol{H}$. However, photons only have two polarizations. The 3D waveguide model uses two field components A_x and A_y corresponding to the two polarizations. The first part of this report provides a step-by-step explanation of how six field components of Maxwell's equations are reduced to two field components. First, the electric field and magnetic field are replaced by four field components: the scalar potential and vector potential. Gauge transformation eliminates the two field components: the scalar potential and the z component of

the vector potential. Finally, Maxwell's equations are reduced to a coupled-wave equation for A_x and A_y.

For EUV lithography simulations, the 3D waveguide model can be further simplified [10–13]. In optical fiber theory, the weakly guiding approximation [14] decomposes all polarization modes into uncoupled linearly polarized modes. This approximation is possible because the refractive index of the core is close to that of the cladding. Similarly, the refractive index of the Ta absorber used in EUV masks is close to that of the vacuum. In the second part of this report, we apply the weakly guiding approximation to the 3D waveguide model. We decompose the coupled vector wave equation of two polarizations into two independent scalar wave equations. Maxwell's equations are simplified to a set of scalar wave equations.

In Section 2 we explain the 3D waveguide model. In Section 3 we apply the 3D waveguide model to EUV lithography simulation. In Section 4 we verify the validity of the weakly guiding approximation. Section 5 is the summary.

2. 3D WAVEGUIDE MODEL

This section explains the basics of the 3D waveguide model.

A. Wave Equation of Vector Potential in Dielectric Materials

In this subsection we derive wave equations in dielectric materials. The dielectric constant ε varies with location. We assume that the materials are nonmagnetic and the magnetic permeability $\mu = 1$. This assumption applies to the materials used in EUV masks. Then, Maxwell's equations are written as follows (Eq. (6.28) in Ref. [15]):

$$\nabla \times \boldsymbol{E} = -\frac{1}{c}\frac{\partial \boldsymbol{H}}{\partial t}, \tag{1}$$

$$\nabla \times \boldsymbol{H} = \frac{4\pi}{c}\boldsymbol{J} + \frac{1}{c}\frac{\partial(\varepsilon \boldsymbol{E})}{\partial t}, \tag{2}$$

$$\nabla \cdot (\varepsilon \boldsymbol{E}) = 4\pi\rho, \tag{3}$$

$$\nabla \cdot \boldsymbol{H} = 0, \tag{4}$$

where c is the speed of the light, and ρ and $\boldsymbol{J}$ are the charge density and the current density, respectively. The charge density and the current density obey the following continuity equation:

$$\frac{\partial \rho}{\partial t} + \nabla \cdot \boldsymbol{J} = 0. \tag{5}$$

The Ohm's law gives the relationship between the electric field and the current density:

$$\boldsymbol{J} = \sigma \boldsymbol{E}, \tag{6}$$

where σ is the conductivity.

We define the plane wave by $\exp(\mathrm{i}(\boldsymbol{k}\cdot\boldsymbol{x} - \omega t))$, where $\boldsymbol{k}$ is the wave vector and ω is the angular velocity. The wave number k is related to the angular velocity by $k = \omega/c$. In steady state for incoming and outgoing waves, $\boldsymbol{E}$, $\boldsymbol{H}$, $\boldsymbol{J}$, and ρ have the same time dependence $\exp(-\mathrm{i}\omega t)$. Then, Maxwell's equations are simplified as follows:

$$\nabla \times \boldsymbol{E} = \mathrm{i}k\boldsymbol{H}, \tag{7}$$

$$\nabla \times \boldsymbol{H} = -\mathrm{i}k\hat{\varepsilon}\boldsymbol{E}, \tag{8}$$

$$\nabla \cdot (\hat{\varepsilon}\boldsymbol{E}) = 0, \tag{9}$$

$$\nabla \cdot \boldsymbol{H} = 0, \tag{10}$$

where $\hat{\varepsilon}$ is the complex dielectric constant defined by

$$\hat{\varepsilon} = \varepsilon + i\frac{4\pi\sigma}{\omega}. \tag{11}$$

Maxwell's equations have six field components $\boldsymbol{E}$ and $\boldsymbol{H}$. We reduce the number to four by using the vector potential $\boldsymbol{A}$ and the scalar potential φ. For an explanation of vector and scalar potentials and their gauge transformation, see Secs. 6.4-5 in Ref. [15].

From Eq. (10) we can define the magnetic field in terms of a vector potential:

$$\boldsymbol{H} = \nabla \times \boldsymbol{A}. \tag{12}$$

Substituting this equation into Eq. (7), we obtain

$$\nabla \times (\boldsymbol{E} - \mathrm{i}k\boldsymbol{A}) = 0. \tag{13}$$

Then, the electric field $\boldsymbol{E}$ is written by using the scalar potential φ as follows:

$$\boldsymbol{E} = \mathrm{i}k\boldsymbol{A} - \nabla\varphi. \tag{14}$$

Equations (8) and (9) are not independent from each other. If $\boldsymbol{E}$ is the solution of Eq. (8), it automatically satisfies Eq. (9). Substituting Eqs. (12) and (14) into Eq. (8), we obtain the following equation:

$$\Delta\boldsymbol{A} + k^2\hat{\varepsilon}\boldsymbol{A} - \nabla(\nabla\cdot\boldsymbol{A}) + \mathrm{i}k\hat{\varepsilon}\nabla\varphi = 0. \tag{15}$$

It is well known that vector potential $\boldsymbol{A}$ and scalar potential φ have gauge transformation freedom. If we change the vector potential $\boldsymbol{A}$ and scalar potential φ simultaneously as follows,

$$\boldsymbol{A} \to \boldsymbol{A} - \nabla\Lambda, \tag{16}$$

$$\varphi \to \varphi - \mathrm{i}k\Lambda, \tag{17}$$

these changes do not affect the observables $\boldsymbol{E}$ and $\boldsymbol{H}$, where Λ is an arbitrary gauge function. This freedom allows applying an additional constraint on $\boldsymbol{A}$ and φ,

$$\nabla\cdot\boldsymbol{A} - \mathrm{i}k\hat{\varepsilon}\varphi = 0, \tag{18}$$

which is called the Lorenz condition.

Inserting the above equation into Eq. (15), we obtain the Helmholtz type wave equation [16] of the vector potential $\boldsymbol{A}$ as follows:

$$\Delta\boldsymbol{A} + k^2\hat{\varepsilon}\boldsymbol{A} - \nabla(\log\hat{\varepsilon})\nabla\cdot\boldsymbol{A} = 0. \tag{19}$$

The Lorenz condition eliminates the scalar potential from the equation. The number of the field components is reduced to three. When the complex dielectric constant $\hat{\varepsilon}$ is not spatially

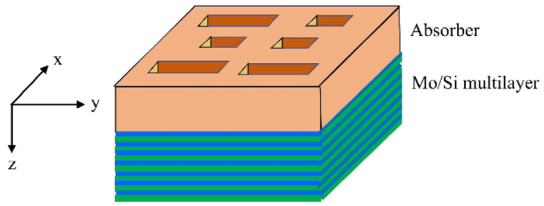

Fig. 1. Cross section of an EUV mask.

uniform, the third term in this equation does not allow solving A_x, A_y, and A_z independently.

B. Coupled-Wave Equations Inside a Layer

In this subsection, we simplify the wave equations, Eq. (17), inside a layer where the complex dielectric constant $\hat{\varepsilon}$ is uniform in the z direction. We still assume that $\hat{\varepsilon}$ depends on x and y. The structure of EUV masks satisfies these assumptions (Fig. 1). For simplicity we assume that the absorber is a single layer. Both inside the absorber layer and Mo/Si multilayers, the complex dielectric constant $\hat{\varepsilon}$ is uniform in the z direction. Inside each layer the z component of the wave equation is written as follows:

$$\Delta A_z + k^2 \hat{\varepsilon} A_z = 0. \tag{20}$$

The Lorenz condition, Eq. (18), partially restricts gauge transformation freedom, but not all of them. If the gauge function Λ satisfies the following equation,

$$\Delta \Lambda + k^2 \hat{\varepsilon} \Lambda = 0, \tag{21}$$

then Lorenz condition is automatically fulfilled. Therefore, an arbitrary function Λ that satisfies Eq. (21) can be added to $\boldsymbol{A}$ and φ. We use this gauge transformation freedom to eliminate A_z in Eq. (19). We define the gauge function Λ as follows [8]:

$$\Lambda(x, y, z) = \int_{z_0}^{z} A_z(x, y, z')\mathrm{d}z' + f(x, y), \tag{22}$$

where z_0 is an arbitrary fixed point inside the layer, and $f(x, y)$ is the solution of the following differential equation:

$$\left(\frac{\partial^2}{\partial x^2} + \frac{\partial^2}{\partial y^2}\right) f(x, y) + k^2 \hat{\varepsilon}(x, y) f(x, y) = -\left.\frac{\partial A_z}{\partial z}\right|_{z=z_0}. \tag{23}$$

It can be easily proved that the gauge function Λ satisfies Eq. (21). With this gauge transformation, the z component of the vector potential can be eliminated because, from Eq. (22),

$$\frac{\partial \Lambda}{\partial z} = A_z. \tag{24}$$

After the gauge transformation, Eq. (19) is simplified as follows:

$$\Delta A_x + k^2 \hat{\varepsilon} A_x - \frac{\partial \log \hat{\varepsilon}}{\partial x}\left(\frac{\partial A_x}{\partial x} + \frac{\partial A_y}{\partial y}\right) = 0, \tag{25}$$

$$\Delta A_y + k^2 \hat{\varepsilon} A_y - \frac{\partial \log \hat{\varepsilon}}{\partial y}\left(\frac{\partial A_x}{\partial x} + \frac{\partial A_y}{\partial y}\right) = 0, \tag{26}$$

$$A_z = 0. \tag{27}$$

Maxwell's equations are reduced to coupled-wave equations of the two components of the vector potential A_x and A_y. The electric field and the magnetic field are calculated from the vector potential as follows:

$$\boldsymbol{E} = \mathrm{i}k\boldsymbol{A} + \frac{\mathrm{i}}{k}\nabla\left(\frac{1}{\hat{\varepsilon}}\nabla \cdot \boldsymbol{A}\right), \tag{28}$$

$$\boldsymbol{H} = \nabla \times \boldsymbol{A}. \tag{29}$$

Equations (25) and (26) are further simplified in the case of one-dimensional mask patterns. These equations are decoupled to transverse electric (TE) and transverse magnetic (TM) waves as shown in Appendix B.

Inside the Mo/Si multilayers, $\hat{\varepsilon}$ is uniform in the x and y directions, so Eqs. (25) and (26) can be solved analytically. The computation time is dominated by the time to solve the coupled-wave equation in the absorber layer. In Fig. 1 we assume that the absorber is a single layer. If the absorber has multiple layers, the computation time becomes longer. If the sidewalls of the absorber are sloped, the staircase approximation can be applied, but the computation time will be very long.

C. Boundary Conditions

At the boundary between the jth and $(j+1)$th layers $(z = z_{j+1})$, the following boundary conditions must be imposed on the electric and magnetic fields in the $x - y$ plane:

$$E_x^{j+1}(x, y, z_{j+1}) = E_x^{j}(x, y, z_{j+1}), \tag{30}$$

$$E_y^{j+1}(x, y, z_{j+1}) = E_y^{j}(x, y, z_{j+1}), \tag{31}$$

$$H_x^{j+1}(x, y, z_{j+1}) = H_x^{j}(x, y, z_{j+1}), \tag{32}$$

$$H_y^{j+1}(x, y, z_{j+1}) = H_y^{j}(x, y, z_{j+1}). \tag{33}$$

We calculate the electric field and the magnetic field within each layer by solving the coupled-wave equations, Eqs. (25) and (26). These equations contain two field components, A_x and A_y. Four boundary conditions, Eqs. (30)–(33), are required to fix the waves going forward A_x^+ and A_y^+, and the waves going backward A_x^- and A_y^-.

D. Incoming and Outgoing Waves in Vacuum

EUV masks are placed inside vacuum where the complex dielectric constant $\hat{\varepsilon}$ is 1. The solution of the wave equation, Eq. (19), is a plane wave $\boldsymbol{A}(\boldsymbol{x}) = \boldsymbol{A}_0 \exp(\mathrm{i}\boldsymbol{k} \cdot \boldsymbol{x})$. From Eqs. (28) and (29), the electric field $\boldsymbol{E}$ and the magnetic field $\boldsymbol{H}$ of the incoming and outgoing waves in vacuum can be described using the vector potential $\boldsymbol{A}$ as follows:

$$\boldsymbol{E} = \mathrm{i}k\boldsymbol{A} - \frac{\mathrm{i}}{k}(\boldsymbol{k} \cdot \boldsymbol{A})\,\boldsymbol{k}, \tag{34}$$

$$\boldsymbol{H} = \mathrm{i}\boldsymbol{k} \times \boldsymbol{A}. \tag{35}$$

The wave vector, electric field, and magnetic field are perpendicular to each other:

$$\boldsymbol{E}\cdot\boldsymbol{k}=\boldsymbol{H}\cdot\boldsymbol{k}=\boldsymbol{E}\cdot\boldsymbol{H}=0. \tag{36}$$

The magnitudes of the electric field and magnetic field are the same:

$$|\boldsymbol{E}|^2=|\boldsymbol{H}|^2=k^2|\boldsymbol{A}|^2-|\boldsymbol{k}\cdot\boldsymbol{A}|^2. \tag{37}$$

Gauge transformation freedom allows us to fix A_z to be zero if the media is uniform in the z direction. This gauge condition can also be applied in vacuum. Therefore, two components of the vector potential, A_x and A_y, determine the electromagnetic field of the light. We call these two components A_x and A_y polarizations. The vector potential, electric field, and magnetic field of the A_x and A_y polarizations are explicitly written as follows.

A_x polarization:

$$\boldsymbol{A}=(A_x,0,0)\,, \tag{38}$$

$$\boldsymbol{E}=\frac{\mathrm{i}A_x}{k}\left(k^2-k_x^2,-k_yk_x,-k_zk_x\right), \tag{39}$$

$$\boldsymbol{H}=\mathrm{i}A_x\left(0,k_z,-k_y\right). \tag{40}$$

A_y polarization:

$$\boldsymbol{A}=\left(0,A_y,0\right), \tag{41}$$

$$\boldsymbol{E}=\frac{\mathrm{i}A_y}{k}\left(-k_xk_y,k^2-k_y^2,-k_zk_y\right), \tag{42}$$

$$\boldsymbol{H}=\mathrm{i}A_y\left(-k_z,0,k_x\right). \tag{43}$$

Figure 2 shows schematic views of A_x and A_y polarizations. When the wave vector is in the $x-z$ plane, $k_y=0$. In this case, A_x polarization corresponds to TM polarization and A_y polarization corresponds to TE polarization. In the same way, when the wave vector is in the $y-z$ plane, A_x polarization corresponds to TE polarization and A_y polarization corresponds to TM polarization.

When $k_x, k_y \ll k$, $\boldsymbol{E}\sim(\mathrm{i}kA_x,0,0)$ for A_x polarization and $\boldsymbol{E}\sim(0,\mathrm{i}kA_y,0)$ for A_y polarization. The electric field for A_x polarization is approximately parallel to the x axis, and the electric field for A_y polarization is approximately parallel to the y axis.

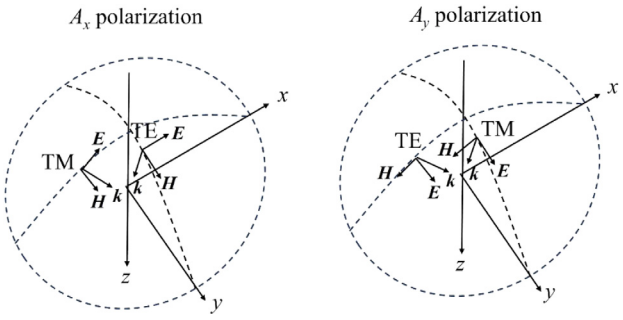

Fig. 2. Schematic views of A_x and A_y polarizations.

3. APPLICATION TO EUV LITHOGRAPHY SIMULATION

In this section we apply 3D waveguide model to EUV lithography simulation.

A. Image Intensity on a Wafer

EUV scanners use Koehler illumination and partial-coherent optics [17] like microscopes. EUV wavelength $\lambda=13.5$ nm. The magnification of the current EUV scanner is $1/4$, and the NA is 0.33. According to Abbe's theory [17], the total image intensity on a wafer, I, is calculated by the incoherent sum of the image intensities illuminated by all points of the effective source S as follows:

$$I(x,y)=\iint S(s_x,s_y)\left|\iint \boldsymbol{E}(\boldsymbol{k}_{\mathrm{out}};\boldsymbol{k}_{\mathrm{in}})P(p_x,p_y)\times e^{i(p_xx+p_yy)}\mathrm{d}p_x\mathrm{d}p_y\right|^2\mathrm{d}s_x\mathrm{d}s_y, \tag{44}$$

where P is the pupil function of the projection optics. The electric field $\boldsymbol{E}$ diffracted by an EUV mask is calculated by solving the 3D waveguide model in Section 2. It depends on the incoming wavevector $\boldsymbol{k}_{\mathrm{in}}$ and the outgoing wavevector $\boldsymbol{k}_{\mathrm{out}}$. These are calculated using the source position of the incoming wave (s_x,s_y) and the pupil position of the outgoing wave (p_x,p_y) as follows:

$$\boldsymbol{k}_{\mathrm{in}}=\left(s_x,-k\sin\theta+s_y,\sqrt{k^2-s_x^2-(-k\sin\theta+s_y)^2}\right), \tag{45}$$

$$\boldsymbol{k}_{\mathrm{out}}=\left(p_x,-k\sin\theta+p_y,-\sqrt{k^2-p_x^2-(-k\sin\theta+p_y)^2}\right). \tag{46}$$

The optics of EUV scanners is reflective, and the chief ray is tilted $\theta=6$ deg in the negative y direction.

We calculate the intensity of the electric field because the photoresist chemically reacts with the electric field. The pupil position is limited by the radius of the pupil defined by NA. The pupil function may include aberrations such as defocus.

B. Polarization Dependence of the Image Intensity

The image intensity depends on the polarization of the incoming wave. We calculate the image intensity of a mask (Fig. 3) that mimics the imec N3 metal layer [18]. The line width is 56 nm on the mask and 14 nm on the wafer. The simulation uses the following optical settings: λ 13.5 nm, NA 0.33, and dipole illumination $\sigma_{\mathrm{out}}/\sigma_{\mathrm{in}}=0.9/0.55$ with the opening angle 90 deg. We assume a conventional Ta absorber of 60 nm thickness and a periodic boundary condition with the period length $L=2048$ nm. The size of the mask area is 2048 nm × 2048 nm. The computational time to solve the 3D waveguide model in this area is 2850 s using Intel Core i9-10920X CPU and Nvidia RTX3090 GPU. We use the MAGMA library [19] to speed up the eigenvalue calculation in Eq. (A16). The calculation time highly depends on the cutoff

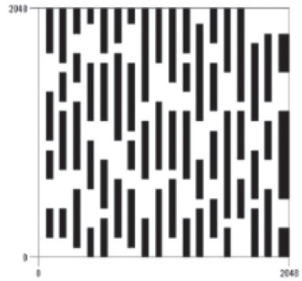

Fig. 3. Mask layout used in the simulation.

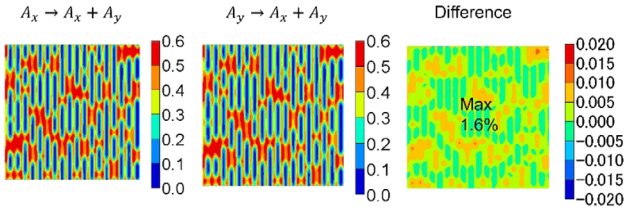

Fig. 4. Image intensities of incoming waves with A_x and A_y polarizations.

momentum. According to Ref. [11], we include the momentum (k_x, k_y), which satisfies

$$\left(\frac{|k_x|}{k_x^{\max}} + 1\right)\left(\frac{|k_y|}{k_y^{\max}} + 1\right) \le 2, \tag{47}$$

where $k_x^{\max} = k_y^{\max} = 6 \cdot \mathrm{NA}/4 \cdot 2\pi/\lambda$. This number is six times larger than the size of the pupil $\mathrm{NA}/4 \cdot 2\pi/\lambda$. When the momentum is discretized by $2\pi/L$, there are 8705 (k_x, k_y) pairs that satisfy Eq. (47). The size of the matrix solving the coupled-wave equations is $17{,}410 \times 17{,}410$ because there are two polarizations.

The region in Eq. (47) is a quasi-hyperbola that mimics the diffraction spectrum of a mask pattern consisting of vertical and horizontal lines or holes. Mask patterns are conventionally designed using X–Y coordinates. The minimum pattern pitch in the X or Y direction is small compared to the minimum pattern pitch in the diagonal direction. Therefore, in momentum space, the diffraction amplitude in the diagonal direction decreases rapidly compared to the amplitude in the X or Y direction.

Figure 4 compares the image intensities of incoming waves with A_x and A_y polarizations. There is a small difference between the two intensities, at most 1.6%. The number is an absolute value relative to the ML reflectance of 0.64. This is because the incident angle is tilted 6 deg in the y direction. In the case of the unpolarized light, the image intensity can be calculated averaging the image intensities of two polarized incoming waves.

Even when the incoming wave has A_x (or A_y) polarization, the outgoing wave has both A_x and A_y polarizations. Figure 5 shows the influence of the polarization change between the incoming wave and outgoing wave. At the middle of Fig. 5, we artificially remove the outgoing wave, which has a different polarization from that of the incoming wave. The contribution of the polarization change is very small, less than 0.01%.

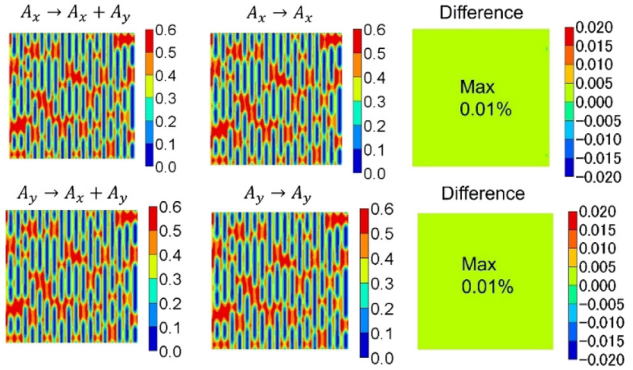

Fig. 5. Influence of the polarization change between the incoming wave and outgoing wave.

4. WEAKLY GUIDING APPROXIMATION

In optical fiber theory, the weakly guiding approximation [14] is often used because the refractive index of the core is close to that of the cladding. The weakly guiding approximation ignores the small cross term that appears in the coupled-wave equation of the transverse electric field [20]. The cross term includes the derivative of the dielectric constant, which is proportional to the difference in refractive index between the core and cladding. In this way, the weakly guiding approximation decomposes the coupled vector wave equation of the electromagnetic field into uncoupled scalar wave equations.

The complex refractive index of the Ta absorber is $(n, k) = \sqrt{\hat{\varepsilon}} = (0.9567, 0.0343)$ [21], which is close to the refractive index of vacuum, 1. The weakly guiding approximation can be applied to EUV masks when the Ta absorber is used. This is the reason that the polarization change from the incoming wave to the outgoing wave is small. According to the weakly guiding approximation, the coupled vector wave equations of two polarizations, Eqs. (25) and (26), are decomposed into the two scalar wave equations as follows:

$$\Delta A_x + k^2 \hat{\varepsilon} A_x - \frac{\partial \log \hat{\varepsilon}}{\partial x}\frac{\partial A_x}{\partial x} = 0, \tag{48}$$

$$\Delta A_y + k^2 \hat{\varepsilon} A_y - \frac{\partial \log \hat{\varepsilon}}{\partial y}\frac{\partial A_y}{\partial y} = 0. \tag{49}$$

The third terms in these equations are small and could be removed, but we retain these terms because they do not affect to the speed of the computation.

Each equation requires two boundary conditions for the waves going forward and backward. Since the electric field of the A_x polarization is approximately parallel to the x axis, we impose the following two boundary conditions on the A_x polarization:

$$E_x^{j+1}(x, y, z_{j+1}) = E_x^{j}(x, y, z_{j+1}), \tag{50}$$

$$H_y^{j+1}(x, y, z_{j+1}) = H_y^{j}(x, y, z_{j+1}). \tag{51}$$

In the same way, we impose the following two boundary conditions on the A_y polarization:

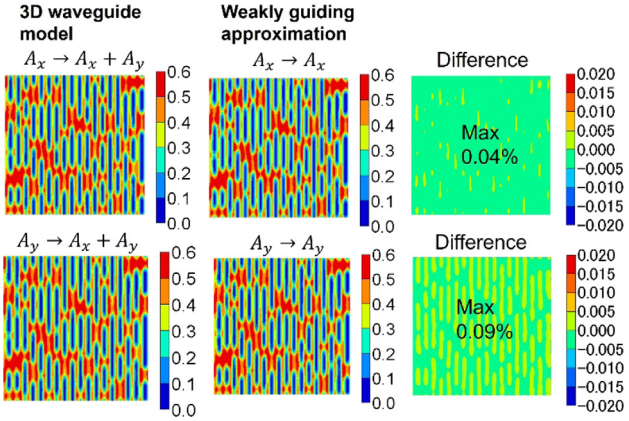

Fig. 6. Comparison of 3D waveguide model and weakly guiding approximation. Ta absorber with 60 nm thickness is used.

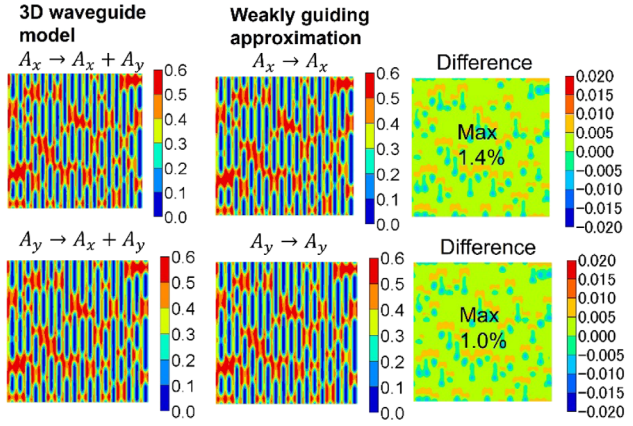

Fig. 7. Comparison of the 3D waveguide model and the weakly guiding approximation. A low-n absorber, TP1, with 45 nm thickness is used.

$$E_y^{j+1}(x, y, z_{j+1}) = E_y^j(x, y, z_{j+1}), \tag{52}$$

$$H_x^{j+1}(x, y, z_{j+1}) = H_x^j(x, y, z_{j+1}). \tag{53}$$

Each equation can be solved independently, and it takes 289 s for a mask area of 2048 nm × 2048 nm. It takes 578 s to solve two equations, which is about 1/5 of the time to solve the original 3D waveguide model.

Figure 6 compares the image intensities calculated by the 3D waveguide model and the weakly guiding approximation. The difference is very small, less than 0.1%. This result is consistent with the results in Fig. 5.

Table 1 summarizes the maximum intensity errors for several test mask patterns, including vertical and horizontal L/S and hole patterns. The illumination used for L/S patterns is dipole illumination, $\sigma_{out}/\sigma_{in} = 0.9/0.55$, with the opening angle 90 deg. The direction of the dipole is perpendicular to the L/S pattern. The illumination used for the hole pattern is annular illumination, $\sigma_{out}/\sigma_{in} = 0.9/0.55$. In all cases the maximum intensity error is less than 0.1%. The accuracy of the weakly guiding approximation is very high when the Ta absorber is used.

Figure 7 shows the results using the low-n absorber TP1 in Ref. [22]. The complex refractive index of the TP1 absorber is (0.91, 0.032). As shown in Fig. 6, the difference between the 3D waveguide model and the weakly guiding approximation increases to 1.4%. The accuracy of the weakly guiding approximation is deteriorated when the low-n absorber is used. Note that the low-n absorber is still under development and the mask process has not yet been established, as discussed in Ref. [22].

5. SUMMARY

We apply the 3D waveguide model to EUV lithography simulation. The 3D waveguide model is equivalent to RCWA. The 3D waveguide model uses two field components of vector potential A_x and A_y. The two field components A_x and A_y correspond to the two polarizations. The electric field of the A_x polarization is approximately parallel to the x axis, and the electric field of the A_y polarization is approximately parallel to the y axis.

The 3D waveguide model solves a coupled vector wave equation for two polarizations. We apply the weakly guiding approximation to the 3D waveguide model. We decompose the vector wave equation of the two polarizations into two independent scalar wave equations. Maxwell's equations are simplified to a set of scalar wave equations. The weakly guiding approximation reduces the computation time to solve the equations. The computation time to solve the weakly guiding approximation is about 1/5 of the time to solve the original 3D waveguide model.

APPENDIX A: EQUIVALENCE BETWEEN 3D WAVEGUIDE MODEL AND RCWA

In this appendix we verify that the 3D waveguide model is equivalent to RCWA.

1. RCWA Formulation

According to the RCWA formulation in Ref. [7], Maxwell's equations are reduced to the following coupled first order differential equations of E_x, E_y, H_x and H_y:

Table 1. Maximum Image Intensity Errors between the 3D Waveguide Model and Weakly Guiding Approximation

Incoming Wave	V L/S L 14 nm P 28 nm	V L/S L 14 nm P 42 nm	V L/S L 20 nm P 40 nm	H L/S L 14 nm P 28 nm	H L/S L 14 nm P 42 nm	H L/S L 20 nm P 40 nm	Hole H 20 nm P 40 nm	Hole H 20 nm P 80 nm
Ax	0.05%	0.01%	0.02%	0.004%	0.01%	0.008%	0.01%	0.008%
Ay	0.09%	0.05%	0.05%	0.07%	0.1%	0.09%	0.03%	0.02%

$$\begin{bmatrix} \partial S_y/\partial(z') \\ \partial S_x/\partial(z') \\ \partial U_y/\partial(z') \\ \partial U_x/\partial(z') \end{bmatrix} = \begin{bmatrix} 0 & 0 & \hat{K}_y\hat{E}^{-1}\hat{K}_x & \hat{I}-\hat{K}_y\hat{E}^{-1}\hat{K}_y \\ 0 & 0 & \hat{K}_x\hat{E}^{-1}\hat{K}_x-\hat{I} & -\hat{K}_x\hat{E}^{-1}\hat{K}_y \\ \hat{K}_x\hat{K}_y & \hat{E}-\hat{K}_y^2 & 0 & 0 \\ \hat{K}_x^2-\hat{E} & -\hat{K}_x\hat{K}_y & 0 & 0 \end{bmatrix} \begin{bmatrix} S_y \\ S_x \\ U_y \\ U_x \end{bmatrix}, \tag{A1}$$

where $\boldsymbol{S}$ and $\boldsymbol{U}$ are the Fourier components of the electric and magnetic fields defined by

$$E_x(x,y,z) = \sum_{m,n} S_x^{mn}(z) \exp\left[\mathrm{i}\left(k_x^m x + k_y^n y\right)\right], \tag{A2}$$

$$E_y(x,y,z) = \sum_{m,n} S_y^{mn}(z) \exp\left[\mathrm{i}\left(k_x^m x + k_y^n y\right)\right], \tag{A3}$$

$$H_x(x,y,z) = \mathrm{i}\sum_{m,n} U_x^{mn}(z) \exp\left[\mathrm{i}\left(k_x^m x + k_y^n y\right)\right], \tag{A4}$$

$$H_y(x,y,z) = \mathrm{i}\sum_{m,n} U_y^{mn}(z) \exp\left[\mathrm{i}\left(k_x^m x + k_y^n y\right)\right]. \tag{A5}$$

The wave vectors for the mth component in the x direction and the nth component in the y direction are written as follows:

$$k_x^m = k_x + m\frac{2\pi}{\Lambda_x}, \tag{A6}$$

$$k_y^n = k_y + n\frac{2\pi}{\Lambda_y}, \tag{A7}$$

where Λ_x and Λ_y are the periodic lengths in the $x$and y directions, respectively.

In Eq. (A1) the normalized z coordinate $z' = kz$, and the matrices $\hat{I}$, $\hat{K}_x$, $\hat{K}_y$, and $\hat{E}$ are dimensionless values as follows:

$$(\hat{I})_{mn,m'n'} = \delta_{mm'}\delta_{nn'}, \tag{A8}$$

$$(\hat{K}_x)_{mn,m'n'} = \delta_{mm'}\delta_{nn'}\frac{k_x^m}{k}, \tag{A9}$$

$$(\hat{K}_y)_{mn,m'n'} = \delta_{mm'}\delta_{nn'}\frac{k_y^n}{k}, \tag{A10}$$

$$(\hat{E})_{mn,m'n'} = \hat{\varepsilon}_{m-m'n-n'}, \tag{A11}$$

where the Fourier component of the dielectric constant is defined by

$$\hat{\varepsilon}(x,y) = \sum_{m,n} \hat{\varepsilon}_{mn} \exp\left[\mathrm{i}\left(m\frac{2\pi x}{\Lambda_x} + n\frac{2\pi y}{\Lambda_x}\right)\right]. \tag{A12}$$

From Eq. (A1) we can derive two sets of the second order differential equations as follows:

$$\begin{bmatrix} \partial^2 S_y/\partial(z')^2 \\ \partial^2 S_x/\partial(z')^2 \end{bmatrix} = \begin{bmatrix} \hat{K}_x^2 + \left(\hat{K}_y\hat{E}^{-1}\hat{K}_y - \hat{I}\right)\hat{E} & \hat{K}_y\left(\hat{E}^{-1}\hat{K}_x\hat{E} - \hat{K}_x\right) \\ \hat{K}_x\left(\hat{E}^{-1}\hat{K}_y\hat{E} - \hat{K}_y\right) & \hat{K}_y^2 + \left(\hat{K}_x\hat{E}^{-1}\hat{K}_x - \hat{I}\right)\hat{E} \end{bmatrix} \begin{bmatrix} S_y \\ S_x \end{bmatrix}, \tag{A13}$$

$$\begin{bmatrix} \partial^2 U_y/\partial(z')^2 \\ \partial^2 U_x/\partial(z')^2 \end{bmatrix} = \begin{bmatrix} \hat{K}_y^2 + \hat{E}\left(\hat{K}_x\hat{E}^{-1}\hat{K}_x - \hat{I}\right) & \left(\hat{K}_x - \hat{E}\hat{K}_x\hat{E}^{-1}\right)\hat{K}_y \\ \left(\hat{K}_y - \hat{E}\hat{K}_y\hat{E}^{-1}\right)\hat{K}_x & \hat{K}_x^2 + \hat{E}\left(\hat{K}_y\hat{E}^{-1}\hat{K}_y - \hat{I}\right) \end{bmatrix} \begin{bmatrix} U_y \\ U_x \end{bmatrix}. \tag{A14}$$

The above equations can be solved in terms of the eigenvalues and eigenvectors of the matrices. We do not need to solve both equations because $\boldsymbol{S}$ and $\boldsymbol{U}$ are not independent fields. For example, if we solve Eq. (A13) for the electric field $\boldsymbol{S}$, then the magnetic field $\boldsymbol{U}$ can be calculated by using Eq. (A1) as follows:

$$\begin{bmatrix} U_y \\ U_x \end{bmatrix} = \begin{bmatrix} \hat{K}_y\hat{E}^{-1}\hat{K}_x & \hat{I}-\hat{K}_y\hat{E}^{-1}\hat{K}_y \\ \hat{K}_x\hat{E}^{-1}\hat{K}_x-\hat{I} & -\hat{K}_x\hat{E}^{-1}\hat{K}_y \end{bmatrix}^{-1} \begin{bmatrix} \partial S_y/\partial(z') \\ \partial S_x/\partial(z') \end{bmatrix}. \tag{A15}$$

2. 3D Waveguide Model

In the 3D waveguide model, Eqs. (25) and (26) can be rewritten in the form of an eigenvalue equation as follows:

$$\begin{bmatrix} \partial^2 F_x/\partial(z')^2 \\ \partial^2 F_y/\partial(z')^2 \end{bmatrix} = \begin{bmatrix} \hat{K}_x^2 + \hat{K}_y^2 - \hat{E} - \hat{Z}_x\hat{K}_x & -\hat{Z}_x\hat{K}_y \\ -\hat{Z}_y\hat{K}_x & \hat{K}_x^2 + \hat{K}_y^2 - \hat{E} - \hat{Z}_y\hat{K}_y \end{bmatrix} \begin{bmatrix} F_x \\ F_y \end{bmatrix}, \tag{A16}$$

where $\boldsymbol{F}$ is the Fourier component of the vector potential $\boldsymbol{A}$:

$$A_x(x,y,z) = \frac{\mathrm{i}}{k}\sum_{m,n} F_x^{mn}(z) \exp\left[\mathrm{i}\left(k_x^m x + k_y^n y\right)\right], \tag{A17}$$

$$A_y(x,y,z) = \frac{\mathrm{i}}{k}\sum_{m,n} F_y^{mn}(z) \exp\left[\mathrm{i}\left(k_x^m x + k_y^n y\right)\right]. \tag{A18}$$

In Eq. (A16) two new matrices $\hat{Z}_x$ and $\hat{Z}_y$ appear. They are defined by

$$(\hat{Z}_x)_{mn,m'n'} = \frac{2\pi(m-m')}{k\Lambda_x}(\zeta)_{m-m'n-n'}, \tag{A19}$$

$$(\hat{Z}_y)_{mn,m'n'} = \frac{2\pi\left(n-n'\right)}{k\Lambda_y}(\zeta)_{m-m'n-n'}, \tag{A20}$$

where ζ is the Fourier component of $\log\hat{\varepsilon}$ as follows:

$$\log\hat{\varepsilon}(x,y) = \sum_{m,n}(\zeta)_{mn} \exp\left[\mathrm{i}\left(m\frac{2\pi x}{\Lambda_x} + n\frac{2\pi y}{\Lambda_x}\right)\right]. \tag{A21}$$

The electric field is calculated by Eq. (28), and this equation is expressed in the matrix form as

$$\begin{bmatrix} S_x \\ S_y \end{bmatrix} = \begin{bmatrix} \hat{I} - \hat{K}_x \hat{E}^{-1} \hat{K}_x & -\hat{K}_x \hat{E}^{-1} \hat{K}_y \\ -\hat{K}_y \hat{E}^{-1} \hat{K}_x & \hat{I} - \hat{K}_y \hat{E}^{-1} \hat{K}_y \end{bmatrix} \begin{bmatrix} F_x \\ F_y \end{bmatrix}. \quad \textbf{(A22)}$$

The magnetic field can be simply calculated from Eq. (29).

$$U_x = \partial F_y / \partial z', \quad \textbf{(A23)}$$

$$U_y = -\partial F_x / \partial z'. \quad \textbf{(A24)}$$

We can verify that the 3D waveguide model is equivalent to RCWA. Differentiating Eq. (A16) by z' and using Eqs. (A23) and (A24) we get

$$\begin{bmatrix} \partial^2 U_y / \partial (z')^2 \\ \partial^2 U_x / \partial (z')^2 \end{bmatrix} = \begin{bmatrix} \hat{K}_x^2 + \hat{K}_y^2 - \hat{E} - \hat{Z}_x \hat{K}_x & \hat{Z}_x \hat{K}_y \\ \hat{Z}_y \hat{K}_x & \hat{K}_x^2 + \hat{K}_y^2 - \hat{E} - \hat{Z}_y \hat{K}_y \end{bmatrix} \begin{bmatrix} U_y \\ U_x \end{bmatrix}. \quad \textbf{(A25)}$$

This equation is identical to Eq. (A14) because

$$\hat{\varepsilon} \frac{\partial}{\partial x} \left(\frac{1}{\hat{\varepsilon}} \frac{\partial}{\partial x} \right) = \frac{\partial^2}{\partial x^2} - \frac{\partial \log \hat{\varepsilon}}{\partial x} \frac{\partial}{\partial x}, \quad \textbf{(A26)}$$

and its matrix representation is

$$\hat{E} \hat{K}_x \hat{E}^{-1} \hat{K}_x = \hat{K}_x^2 - \hat{Z}_x \hat{K}_x. \quad \textbf{(A27)}$$

APPENDIX B: ONE-DIMENSIONAL MASK PATTERN

If the mask pattern is uniform in the y direction and the incoming wave is in the $x-z$ plane, $\hat{\varepsilon}$, A_x, and A_y do not depend on the y coordinate. In this case, Eqs. (25) and (26) are further simplified as follows:

$$\frac{\partial^2 A_x}{\partial x^2} + \frac{\partial^2 A_x}{\partial z^2} + k^2 \hat{\varepsilon} A_x - \frac{\partial \log \hat{\varepsilon}}{\partial x} \frac{\partial A_x}{\partial x} = 0, \quad \textbf{(B1)}$$

$$\frac{\partial^2 A_y}{\partial x^2} + \frac{\partial^2 A_y}{\partial z^2} + k^2 \hat{\varepsilon} A_y = 0. \quad \textbf{(B2)}$$

The above two equations can be solved independently. The general solution is given by a combination of the following two special solutions:

I) $A_x = 0$, $A_y \neq 0$, $A_z = 0$.

From Eqs. (28) and (29) the electric and magnetic fields are

$$\boldsymbol{E} = (0, ikA_y, 0), \quad \textbf{(B3)}$$

$$\boldsymbol{H} = \left(-\frac{\partial A_y}{\partial z}, 0, \frac{\partial A_y}{\partial x} \right). \quad \textbf{(B4)}$$

Replacing the field from A_y to E_y,

$$E_y = \mathrm{i} k A_y. \quad \textbf{(B5)}$$

Equations (B2)–(B4) are rewritten as follows:

$$\frac{\partial^2 E_y}{\partial x^2} + \frac{\partial^2 E_y}{\partial z^2} + k^2 \hat{\varepsilon} E_y = 0, \quad \textbf{(B6)}$$

$$\boldsymbol{E} = \left(0, E_y, 0\right), \quad \textbf{(B7)}$$

$$\boldsymbol{H} = \left(\frac{\mathrm{i}}{k} \frac{\partial E_y}{\partial z}, 0, -\frac{\mathrm{i}}{k} \frac{\partial E_y}{\partial x} \right). \quad \textbf{(B8)}$$

The solution is known to be a TE wave:

II) $A_x \neq 0$, $A_y = 0$, $A_z = 0$.

From Eqs. (28) and (29) the electric and magnetic fields are

$$\boldsymbol{E} = \left(-\frac{\mathrm{i}}{k\hat{\varepsilon}} \frac{\partial^2 A_x}{\partial z^2}, 0, \frac{\mathrm{i}}{k\hat{\varepsilon}} \frac{\partial^2 A_x}{\partial z \partial x} \right), \quad \textbf{(B9)}$$

$$\boldsymbol{H} = \left(0, \frac{\partial A_x}{\partial z}, 0 \right). \quad \textbf{(B10)}$$

Replacing the field from A_x to H_y,

$$H_y = \frac{\partial A_x}{\partial z}. \quad \textbf{(B11)}$$

Equations (B1), (B9), and (B10) are rewritten as follows:

$$\frac{\partial^2 H_y}{\partial x^2} + \frac{\partial^2 H_y}{\partial z^2} + k^2 \hat{\varepsilon} H_y - \frac{\partial \log \hat{\varepsilon}}{\partial x} \frac{\partial H_y}{\partial x} = 0, \quad \textbf{(B12)}$$

$$\boldsymbol{E} = \left(-\frac{\mathrm{i}}{k\hat{\varepsilon}} \frac{\partial H_y}{\partial z}, 0, \frac{\mathrm{i}}{k\hat{\varepsilon}} \frac{\partial H_y}{\partial x} \right), \quad \textbf{(B13)}$$

$$\boldsymbol{H} = \left(0, H_y, 0\right). \quad \textbf{(B14)}$$

The solution is known to be a TM wave.

Funding. Ministry of Education, Culture, Sports, Science and Technology (MEXT) Initiative to Establish Next-generation Novel Integrated Circuits Centers (X-NICS) (Grant JPJ011438).

Disclosures. The authors declare no conflicts of interest.

Data availability. The data supporting the findings of this study are available within the paper.

REFERENCES

1. V. Philipsen, "Mask is key to unlock full EUV potential," Proc. SPIE **11609**, 1160904 (2021).
2. A. Erdmann, P. Evanschitzky, G. Bottiglieri, *et al.*, "3D mask effects in high NA EUV imaging," Proc. SPIE **10957**, 109570Z (2019).
3. A. Wong and A. Neureuther, "Mask topography effects in projection printing of phase-shifting masks," IEEE Trans. Electron Devices **41**, 895–902 (1994).
4. M. G. Moharam and T. K. Gaylord, "Rigorous coupled-wave analysis of planar-grating diffraction," J. Opt. Soc. Am. **71**, 811–818 (1981).
5. M. G. Moharam, E. B. Grann, and D. A. Pommet, "Formulation for stable and efficient implementation of the rigorous coupled-wave analysis of binary gratings and optics," J. Opt. Soc. Am. A **12**, 1068–1076 (1995).
6. M. G. Moharam, D. A. Pommet, and E. B. Grann, "Stable implementation of the rigorous coupled-wave analysis for surface-relief gratings: enhanced transmittance matrix approach," J. Opt. Soc. Am. A **12**, 1077–1086 (1995).

7. P. C. Logofatu, "Rigorous coupled-wave analysis for two-dimensional gratings," Proc. SPIE **5972**, 59720Q (2005).
8. H. Tanabe, "Modeling of optical images in resists by vector potentials," Proc. SPIE **1674**, 637–649 (1992).
9. K. D. Lucas, H. Tanabe, and A. J. Strojwas, "Efficient and rigorous three-dimensional model for optical lithography simulation," J. Opt. Soc. Am. A **13**, 2187–2199 (1996).
10. H. Tanabe, S. Sato, and A. Takahashi, "Fast EUV lithography simulation using convolutional neural network," J. Micro/Nanopattern. Mater. Metrol. **20**, 041202 (2021).
11. H. Tanabe and A. Takahashi, "Data augmentation in extreme ultraviolet lithography simulation using convolutional neural network," J. Micro/Nanopattern. Mater. Metrol. **21**, 041602 (2022).
12. H. Tanabe, A. Jinguji, and A. Takahashi, "Evaluation of convolutional neural network for fast extreme violet lithography simulation using 3nm node mask patterns," J. Micro/Nanopattern. Mater. Metrol. **22**, 024201 (2023).
13. H. Tanabe, A. Jinguji, and A. Takahashi, "Accelerating extreme ultraviolet lithography simulation with weakly guiding approximation and source position dependent transmission cross coefficient formula," J. Micro/Nanopattern. Mater. Metrol. **23**, 014201 (2024).
14. D. Gloge, "Weakly guiding fibers," Appl. Opt. **10**, 2252–2258 (1971).
15. J. D. Jackson, *Classical Electrodynamics*, 2nd ed. (Wiley, 1975).
16. J. W. Goodman, *Introduction to Fourier Optics* (McGraw-Hill, 1968).
17. M. Born and E. Wolf, *Principles of Optics*, 7th ed. (Cambridge University, 1999).
18. D. Xu, W. Gillijns, L. E. Tan, *et al.*, "Investigation of low-n mask in 0.33 NA EUV single patterning at pitch 28 nm metal design," Proc. SPIE **12051**, 120510H (2022).
19. S. Tomov, J. Dongarra, and M. Baboulin, "Towards dense linear algebra for hybrid GPU accelerated manycore systems," Parallel Comput. **36**, 232–240 (2010).
20. A. W. Snyder and W. R. Young, "Modes of optical waveguide," J. Opt. Soc. Am. **68**, 297–309 (1978).
21. E. Gullikson, "CXRO X-ray database," https://henke.lbl.gov/optical_constants/.
22. S. Lin, C. Lee, Y. Chen, *et al.*, "EUV APSM mask prospects and challenges," Proc. SPIE **12751**, 127510N (2023).